Langmuir

Article

pubs.acs.org/Langmuir

Modulation of the Coffee-Ring Effect in Particle/Surfactant Mixtures: the Importance of Particle−Interface Interactions

Manos Anyfantakis,*[,†] Zheng Geng,[†] Mathieu Morel, Sergii Rudiuk, and Damien Baigl*

Department of Chemistry, Ecole Normale Supérieure-PSL Research University, 24 rue Lhomond, F-75005, Paris, France
Sorbonne Universités, UPMC Univ Paris 06, PASTEUR, F-75005, Paris, France
CNRS, UMR 8640 PASTEUR, F-75005, Paris, France

Supporting Information

ABSTRACT: We study the effect of surfactants on the deposits formed after the evaporation of colloidal suspension drops, at initial concentrations lower than the critical micellar concentrations, for various particle/surfactant mixtures. We show that the surfactant-mediated interactions between particles and the liquid−gas (LG) and liquid−solid (LS) interfaces, rather than the flow patterns, primarily define the morphology of the dry deposit in a robust and reproducible manner. For like-charged particle/surfactant mixtures, most of the particles form a ring-shaped deposit (according to the so-called "Coffee-Ring Effect"), but some particles can also be deposited inside the ring in a way that is modulated by electrostatic interactions between the particles and the LS interface. For oppositely charged systems, surfactant adsorption to the particle surface strongly affects particle-LG interface interactions, which in turn control the deposition pattern. For low surfactant concentrations, coffee-rings are systematically observed. For intermediate concentrations, the charge of surfactant-decorated particles becomes nearly neutral, and their hydrophobicity is enhanced, which promotes particle trapping at the LG interface. A particle skin is formed and its deposition upon drying leads to homogeneous disk-like patterns. For high surfactant concentrations, particle charge is reversed, and coffee-rings are observed again. Notably, this ring-disk-ring evolution of the deposition behavior as a function of surfactant concentration is observed in a variety of mixtures, regardless of particle absolute charge and surface chemistry as well as of surfactant charge and hydrophobicity. Its apparent universal character makes it a promising strategy for a robust control of particle deposition from evaporating drops.

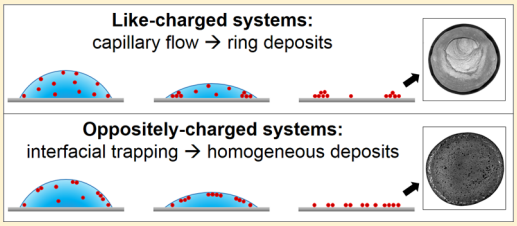

I. INTRODUCTION

Particle deposition from evaporating sessile drops of colloidal suspensions phenomenologically seems to be a rather simple problem. A first surprise comes from the formation of the intuitively unexpected ring-shaped deposits observed in drying drops of spilled coffee. The so-called Coffee-Ring Effect (CRE) was explained based on the evaporation-driven capillary flow of liquid toward the contact line of the drop.[1] This flow is induced by the inhomogeneous evaporation profile along the free interface of a pinned drop with a contact angle of less than 90°. Any dissolved/suspended material in the liquid is transported to the drop edge, yielding the familiar ring patterns.[2] Initiated by the landmark paper of Deegan et al.,[1] the increased interest in the subject further showed that numerous parameters are entangled in a complex problem involving a variety of transport phenomena, length-scales, and time-scales.[3,4] As a consequence, numerous parameters—including flow patterns,[5,6] interactions,[3,7] drying conditions,[8,9] physicochemical properties of solutes,[10] solvents,[11] and substrates[12]—can affect the final deposition pattern. Therefore, the ability to tailor evaporation-driven patterning on solid substrates crucially depends on our level of fundamental understanding of how it proceeds.

Besides its scientific interest, the CRE in particular and evaporative particle deposition in general[13,14] are directly involved in a number of technological applications. The industry of inkjet printing regularly requires uniform deposits after the drying of picoliter ink drops of different compositions jetted on various substrates.[15] In cDNA microarrays, inhomogeneities in the deposit morphology caused by the CRE are a limiting factor in their performance.[16] Hence, many approaches have been utilized to suppress or ideally to control the CRE.[17] The most common strategy to achieve homogeneous solute depositions relies on additives to control the flow patterns within an evaporating drop. Examples include cosolvents[11] and polymers[18] that were reported to create Marangoni flows, as well as nanoparticles[19] that were used to induce a sol−gel transition and therefore control the radial flow in drying picoliter droplets. The shape of the suspended particles was also found to play a crucial role in the deposition morphology. For instance, elimination of the CRE was possible by using suspensions of ellipsoidal particles.[10]

Early experiments by Deegan have shown that surfactants can affect particle deposition during drop drying.[20] In the following studies, surfactants have been frequently employed to

Received: February 4, 2015
Revised: March 19, 2015
Published: March 23, 2015

ACS Publications © 2015 American Chemical Society

DOI: 10.1021/acs.langmuir.5b00453
Langmuir 2015, 31, 4113−4120

control the deposition of various solutes. A central idea behind their use was based on the expectation that solutal Marangoni flows would develop in a pinned sessile drop. The radial outward flow would bring surfactants to the contact line, therefore increasing the local concentration and decreasing the surface tension close to the drop edge. The gradient in surface tension along the liquid−gas (LG) interface should induce a Marangoni flow from the edge to the apex of the drop. This surface flow was expected to push particles away from the contact line and therefore lead to the suppression of the CRE. Kajiya et al. reported that surfactant addition to evaporating polymer solution drops led to flattening of the concentration profile of the final polymer film, owing to a solutal Marangoni flow opposing the radial flow.[21] Deng et al. showed that the ring structure frequently observed in protein microarrays could be eliminated by nonionic surfactants.[22] The authors explained that surfactants displaced proteins that otherwise tended to adsorb at the LG interface and be transported to the periphery of the drop. Still et al. reported that Marangoni eddies developing in drying colloidal drops prevented particles from reaching the contact line, leading to more uniform depositions when surfactant concentrations were above the critical micellar concentrations (CMC).[23] Interestingly, secreted biosurfactants were shown to lead to homogeneous bacteria distribution from drying drops, ascribed to Marangoni stresses reversing the radial capillary flow.[24] Truskett and Stebe sprayed insoluble surfactant onto a drop and demonstrated a variety of patterns depending on the state of the surfactant monolayer at the LG interface.[25] Homogeneous deposits were also achieved, and their formation was attributed to an increase in surfactant concentration near the contact line, which was proposed to retard evaporation close to the drop edge.

Besides affecting the flow patterns, surfactants can influence the particle−particle, particle−free interface, and particle−substrate interactions. The effect of such interactions on particle deposition from evaporating drops has been in general overlooked by the majority of the published works, with, however, a few notable exceptions. Yan et al. studied the effect of particle and substrate charge as well as of surfactant addition on colloidal self-assembly in sessile drops.[26] Ordered and disordered assemblies were explained based on the electrostatic and hydrophobic interactions between the colloids, the surfactants and the liquid−solid (LS) interface. Crivoi and Duan investigated the drying of drops containing aggregating aluminum oxide nanoparticles. Surfactant-free suspensions led to patterns of uniform coverage, while addition of surfactant promoted the formation of coffee-rings. The authors underlined that particle sticking probability was a decisive factor affecting the deposit morphology.[27] Recently, we demonstrated that light could effectively control the CRE by tuning the interactions between particles and their affinity to the LG interface when cationic photosensitive surfactants and anionic colloids were mixed.[28] All these results emphasized the effect of interactions between particles and interfaces on the pattern formation from evaporating suspension drops of specific formulations. Knowing that surfactants can strongly affect particle surface properties and therefore modify their behavior at interfaces, we hypothesized that they can control the CRE even at very low concentrations, through interaction modifications rather than affecting the flow patterns. However, to our knowledge, a systematic investigation of the role of surfactants on particle deposition below CMC has yet to be done.

Here, we study the effect of various standard surfactants on the morphology of deposits obtained from evaporating drops of different particle suspensions, at surfactant concentrations lower than the CMC. Deposits ranging from typical coffee rings to fully homogeneous disk-shaped patterns were observed depending on the surfactant concentration and the charge of the particle/surfactant system. The observed morphologies are explained considering the interactions between the particles and the liquid−solid and liquid−gas interfaces, which are mediated by the amount of surfactants being adsorbed on the particle surface. The observed phenomenology is confirmed in different particle/surfactant systems, pointing toward a universal mechanism of surfactant-directed particle deposition.

II. MATERIALS AND METHODS

Materials. Milli-Q water (Millipore) was used for all experiments. The anionic polystyrene particles (PS-AA, diameter: 500 nm) contained surface groups of acrylic acid[29] and were kindly provided by the group of Prof. U. Jonas (University of Siegen, Germany). The cationic polystyrene particles (PS-AMI, diameter: 510 nm) contained amidine surface groups and were purchased from Life Technologies (amidine latex, catalogue number: A37317). Both dispersions were surfactant-free. Dodecyltrimethylammonium bromide (DTAB, purity ≥98%, Sigma), hexadecyltrimethylammonium bromide (CTAB, purity ≥99%, Sigma), sodium dodecyl sulfate (SDS, purity ≥99%, Fluka), sodium dodecylbenzenesulfonate (SDBS, certified purity 49.7% as Carbon, Fluka) and poly-L-lysine hydrobromide (Sigma) were used as received.

Sample Preparation and Drop Deposition. For sample preparation, the proper amounts of water, concentrated surfactant solution, and concentrated particle suspension were added in this order in an Eppendorf tube. After mixing with a micropipette (Eppendorf), the suspension was vortexed for 1 min. Before each experiment, the suspensions were mixed for about 15 s, sonicated in an ultrasound bath for 1 min, and mixed again for 1 min. A drop (0.8 μL) was then immediately deposited on the substrate using a micropipette and was covered with a box to avoid air currents, except for obtaining real-time videos (Figure 5, Supporting Information Figure S5, and Videos S1−S4) where no box and smaller drops (0.5 μL) were used. All drying experiments were performed at 22.7 ± 1 °C.

The employed substrates were glass coverslips (Menzel-Gläser) used as received for all experiments except those corresponding to Figure S3c−d. In the latter case, the glass coverslips were rendered positively charged by a poly-L-lysine coating, performed as follows. First, the coverslips were plasma-cleaned for 3 min (550 mTorr air) in order to achieve a high density of silanol groups on the glass surface. Then, they were placed on a Petri dish and were covered with 375 μL of a 0.5 g/L poly-L-lysine solution containing 100 mM of NaCl. A few water drops were placed adjacent to the coverslips, and the Petri dish was closed in order to ensure a saturated atmosphere and avoid significant solution evaporation. The substrates were left for about 18 h for the adsorption to occur. Afterward, the substrates were immersed in water for 1 h and rinsed with copious amounts of water to ensure removal of nonadsorbed polymer chains.

Contact Angle of Milli-Q Water on Glass Coverslips. Milli-Q water partially wets the glass coverslips we used as substrates. We measured a static contact angle of θ = 55.5 ± 2° (mean value ± standard deviation of 19 measurements using two different coverslips).

Imaging of the Deposits. Transmitted brightfield images of the deposited patterns and videos of the evaporating processes were captured with an inverted optical microscope (Zeiss Axio Observer) equipped with an EMCCD camera (PhotonMax 512, Princeton Instruments). Köhler illumination conditions were set prior to experiments. All images were acquired in similar illumination conditions and acquisition settings. They are displayed without any postprocessing.

Measurement of the Effective Surface Potential (ζ) of the Particles. Mixtures held in Eppendorf tubes were shortly vortexed (15

DOI: 10.1021/acs.langmuir.5b00453
Langmuir 2015, 31, 4113−4120

s), sonicated (1 min) and vortexed again (1 min) prior to being loaded in plastic capillary cells (DTS1070, Malvern Instruments) using a plastic syringe. The particle surface potential was measured utilizing a Zetasizer Nano-ZS (Malvern Instruments). All experiments were performed at 25 °C. Each measurement lasted 60 s and was repeated three times.

III. RESULTS AND DISCUSSION

Suspensions of Anionic Particles: Deposition Patterns. We first explored the effect of surfactants on the patterns deposited by evaporating drops of anionic particle (PS-AA) suspensions. We used the negatively charged surfactant SDS (CMC = 8.1 mM[30]) and two positively charged surfactants DTAB (CMC = 13.4 mM[31]) and CTAB (CMC = 0.92 mM[30]). We prepared particle/surfactant mixtures, keeping the PS-AA concentration constant (2 mg/mL) and varying the surfactant type and concentration. We deposited 0.8 μL drops on glass coverslips, and we observed the patterns obtained after the evaporation was complete (Figure 1). The top row of Figure 1

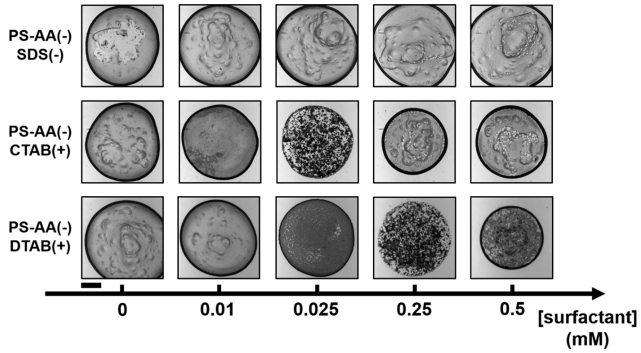

Figure 1. Brightfield microscope images of the deposits formed from evaporating drops (0.8 μL) containing mixtures of anionic PS particles (PS-AA, 500 nm diameter, 2 mg/mL) and anionic (SDS) or cationic (CTAB, DTAB) surfactants at various concentrations. The scale bar is 500 μm.

shows patterns obtained with the mixture PS-AA/SDS, where both particles and surfactants carried a negative charge. For all surfactant concentrations examined (0–0.5 mM), the majority of particles were accumulated at the edge of the drop after drying, forming a typical ring-shaped deposit. Therefore, SDS did not affect the particle distribution profile in the deposit regardless of its concentration (kept below CMC).

The situation changed dramatically when cationic surfactants were mixed with the anionic PS-AA particles. Patterns obtained for PS-AA/CTAB mixtures (Figure 1, middle row) were rings for low surfactant concentrations ([CTAB] = 0–0.01 mM), homogeneous disks for intermediate concentrations ([CTAB] = 0.025 mM), and rings again for the two highest concentrations explored ([CTAB] = 0.25 and 0.5 mM). Drops dispensed from PS-AA/DTAB mixtures showed a qualitatively similar ring-disk-ring evolution with increasing surfactant concentration. However, the intermediate concentrations at which homogeneous disks of similar morphology were observed were shifted to higher values ([DTAB] = 0.25 mM). Profilometry analysis confirmed the ring-disk-ring evolution of the profile morphology as a function of DTAB concentration (Figure S1). The marked difference between the effects of anionic and cationic surfactants on negatively charged particle deposition suggests that electrostatic interactions between surfactants and particles play a key role in the formation of the particle pattern upon drop evaporation.

Suspensions of Anionic Particles: Zeta Potential. In order to characterize the surfactant/particle interaction, we measured the zeta potential (ζ) of their mixtures (Figure 2).

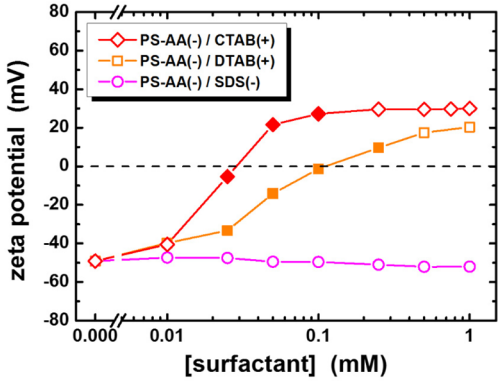

Figure 2. Zeta potential measurements of mixtures of anionic PS particles (PS-AA, 500 nm diameter, 2 mg/mL) with anionic (SDS) or cationic (DTAB, CTAB) surfactants at various concentrations. Symbols represent mean values of three independent measurements. The error bars (standard deviation) were smaller than the symbol size and are not shown here. Open and filled symbols correspond to deposits with ring-shaped and disk-shaped morphology, respectively.

Since the surfactant concentration was always below or close to CMC, we can consider that the main contribution to ζ came from the particle surface, the charge of which could be affected by the adsorption of surfactants. For the PS-AA suspensions containing no surfactants, we measured $\zeta = -50$ mV, indicating well-stabilized suspensions due to the negative charges at the particle surface. ζ did not significantly change upon addition of SDS, showing that surfactant adsorption on the particle surface was negligible in this case. This is expected owing to the electrostatic repulsion between the negatively charged polar head of SDS and the anionic PS-AA particles. On the contrary, for the PS-AA/CTAB system, ζ increased with increasing [CTAB], became almost 0 mV for [CTAB] = 0.025 mM and reached a positive plateau value of about +25 mV for [CTAB] > 0.25 mM. Similarly, surface charge neutralization and reversal with increased surfactant concentration were observed for the PS-AA/DTAB mixtures. However, the ζ evolution was less steep with DTAB and the surface charge neutralization was obtained at a much higher DTAB concentration (around 0.1 mM). Both neutralization and charge reversal have been commonly observed in various oppositely charged particle/surfactant systems and are usually attributed to electrostatic and hydrophobic interactions driving surfactant adsorption on the particle surface.[32] A first layer of surfactants is formed by electrostatic adsorption leading to particle charge neutralization while additional adsorption mediated by surfactant–surfactant hydrophobic interactions leads to the charge reversal. The difference between DTAB and CTAB is attributed to the difference in their hydrophobicity, with a stronger and steeper binding for CTAB, which has a lower CMC and therefore a stronger propensity to aggregate.

Moreover, we observed a marked correlation between the ζ evolution and the morphology of the deposited patterns. Strikingly, mixtures displaying highly negative or highly positive ζ values systematically led to ring-shaped patterns, while ζ values close to neutral potential corresponded to disk-like

DOI: 10.1021/acs.langmuir.5b00453
Langmuir 2015, 31, 4113–4120

patterns, regardless of surfactant nature (Figures 2 and S2). These results show that the modification of the particle surface by surfactant adsorption is critical in directing the pattern formation.

Suspensions of Cationic Particles: Deposition Patterns. Given that (i) surfactant binding on the particles was responsible for ζ modifications and that (ii) patterns from evaporating drops were directly linked to the particle surface charge and presence of adsorbed surfactants, we hypothesized that surfactant-mediated deposit homogenization should be generally applicable to any colloidal suspension containing oppositely charged surfactants. In order to test this hypothesis, we prepared mixtures with cationic particles (PS-AMI) at a concentration fixed at 1 mg/mL and an anionic surfactant (SDBS, CMC = 1.6 mM[33]) at various concentrations. We deposited drops of 0.8 μL on glass coverslips, and we observed the patterns after drying (Figure 3).

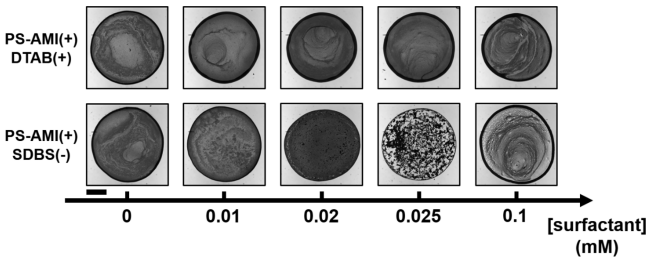

Figure 3. Brightfield microscope images of the deposits formed from evaporating droplets (0.8 μL) of mixtures of cationic PS particles (PS-AMI, 510 nm diameter, 1 mg/mL) with cationic (DTAB) and anionic (SDBS) surfactants. The scale bar is 500 μm.

For the surfactant-free dispersions (Figure 3, left panels), most of the particles were gathered at the position of the contact line upon drying, forming a typical ring pattern. However, a large number of particles were also deposited inside the ring, yielding overall a more homogeneous deposit compared to suspensions of PS-AA (Figure 1). We attribute this effect to Coulomb attractions between the cationic PS-AMI particles and the negatively charged glass substrate. This is supported by experiments performed with positively charged substrates (poly-L-lysine-coated glass) and drops of surfactant-free suspensions of anionic (PS-AA) or cationic (PS-AMI) particles (Figure S3). For PS-AMI suspension drops deposited on the poly-L-lysine-coated glass, a marked ring pattern was observed (Figure S3c) showing that the vast majority of particles migrated to the drop edge. On the contrary, drops from PS-AA suspensions yielded patterns consisting of a ring encircling a quite uniform particle deposit (Figure S3d). In summary, particle−substrate electrostatic attraction (Figure S3a,d) led to coffee rings with a large number of particles within the area enclosed by the ring, whereas repulsive interactions between particles and the substrate (Figure S3b,c) led to typical ring stains, with only few particles deposited at the ring interior.

The bottom row of Figure 3 shows deposits obtained from the mixture of the cationic PS-AMI particles with the anionic surfactant SDBS at various concentrations. The evaporation led to rings for low surfactant concentrations ([SDBS = 0−0.01 mM]), homogeneous disk-shaped deposits for intermediate concentrations (0.02−0.025 mM) and rings again for the highest concentration used (0.1 mM). Interestingly, the ring-disk-ring evolution of the deposit morphology with increasing [SDBS] was observed in this oppositely charged particle/surfactant mixture again, in a way reminiscent of the PS-AA/CTAB and PS-AA/DTAB systems (Figure 1). Conversely, deposits obtained from the like-charged mixture PS-AMI/DTAB (Figure 3, top row) were always rings ([DTAB] = 0−1 mM).

Suspensions of Cationic Particles: Zeta Potential. Figure 4 shows the ζ measurements for the mixtures containing

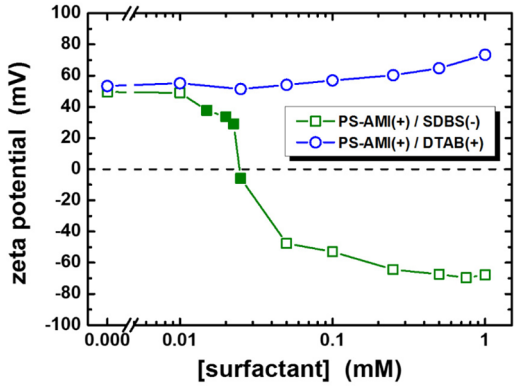

Figure 4. Zeta potential measurements of mixtures of cationic PS particles (PS-AMI, 510 nm diameter, 1 mg/mL) with anionic (SDBS) and cationic (DTAB) surfactants. Symbols represent mean values of three independent measurements. The error bars (standard deviation) were always smaller than the symbol size and are omitted here for clarity. Open and filled symbols correspond to deposits with ring-shaped and disk-shaped morphology, respectively.

PS-AMI particles and anionic (SDBS) or cationic (DTAB) surfactants. For the surfactant-free suspensions, $\zeta \approx +50$ mV, indicating a high density of positive charges at the particle surface. Adding DTAB did not significantly modify ζ, except for the two highest concentrations reported here (0.5 and 1 mM), where ζ slightly increased to ca. +60 mV, possibly due to hydrophobic adsorption of the surfactant on the particle surface. In contrast, SDBS-containing PS-AMI suspensions displayed an [SDBS]-dependent potential. For low [SDBS] (0.01 mM), ζ remained unchanged (about +50 mV); however, upon increasing concentration, ζ decreased and became almost 0 mV at [SDBS] = 0.025 mM. With a further increase in [SDBS], ζ was reversed and decreased down to a plateau value of about −70 mV ([SDBS] = 0.5−1 mM). Again, and in a way similar to the reverse system with anionic particles and cationic surfactants, we observed both the adsorption of surfactants on the particle surface mediated by electrostatic and hydrophobic effects and a correlation between the evolution of ζ and that of the deposit morphology. Rings were observed at low and high ζ values, while disk-shaped deposits were observed for intermediate ζ values around neutral potential (Figure S4). It is also interesting to note that the ring pattern obtained for PS-AMI/SDBS suspensions at highly negative ζ (i.e., high SDBS concentration) contained much less particles at the ring interior than that obtained at highly positive ζ (i.e., low SDBS concentration). We attribute this behavior to the contribution of the electrostatic interactions between the particles and the LS interface, with a stronger adsorption of the particles on the negatively charged glass substrate at the ring interior in the case of particles with positive ζ.

Surfactant-Mediated Particle Trapping at the LG Interface. From the results presented above, it is clear that,

DOI: 10.1021/acs.langmuir.5b00453
Langmuir 2015, 31, 4113−4120

regardless of the system, the degree of adsorption of surfactants on the surface of oppositely charged particles defined both the electrostatic and hydrophobic properties of the particles as well as the morphology of the deposit pattern. In particular, in the case of intermediate surfactant concentrations where ζ had a low absolute value, drop evaporation led to homogeneous patterns. It is reasonable to expect that, besides modification of the electrostatic potential, surfactant adsorption induced a change in the particle hydrophobicity, since the apolar tails of the amphiphilic molecules pointed out of the particle surface. Indeed, it has been shown that, in mixtures of anionic silica nanoparticles with CTAB, the contact angle of the nanoparticles at the oil/water interface was larger at an intermediate range of CTAB concentrations than that for lower and higher CTAB concentrations.[34] The contact angle formed between a particle and a fluid−fluid interface defines the affinity of the former to the latter as well as the strength of the interaction potential.[35] In our experiments, the expected increase in particle hydrophobicity caused by surfactant adsorption, was confirmed by visual observations during sample preparation. Only at intermediate surfactant concentrations corresponding to low absolute value of ζ did we notice the formation of a thin particle layer on the Eppendorf tube walls, denoting particle adsorption at the wall surface by hydrophobic interactions.

For a particle of radius R being adsorbed at a LG interface with surface tension γ_{LG} and forming with it a contact angle θ, the energy E required to bring the particle from the interface to the water phase[35] is $E = \pi R^2 \gamma_{LG}(1 - \cos\theta)^2$. As a consequence, an increase in particle hydrophobicity inducing an increase in θ should be accompanied by an increase in E, therefore increasing the trapping probability of the particles at the LG interface in a drying drop. To test our hypothesis, we employed high-magnification video microscopy, and we focused at the free interface during drop evaporation. Figure 5 shows snapshots during the drying of a 0.5 μL drop containing 1 mg/mL PS-AA particles with 0.025 mM DTAB (a,b), as well as a surfactant-free drop (d,e). To get a better visualization of the particles, we used a particle concentration half that in Figures 1 and 2. The corresponding videos can be found in the Supporting Information (Videos S1, S2). For the snapshots shown here, the part of field of view that was in-focus corresponded to the LG interface (central part of Figure 5a,b,d,e). Figure 5c,f shows low magnification images of the final dry deposits of the two drops.

For the DTAB-containing drop, the formation of extended aggregates (~15 μm) of particles at the LG interface was clearly observed after 150 s (Figure 5a). It is worth noticing that smaller aggregates could be observed at the LG interface soon (i.e., ~10 s) after drop deposition. As evaporation proceeded, individual aggregates were connected to each other at the interface to form a particle skin (Figure 5b). Contrarily to the LG interface, only a few aggregates were observed in the bulk during the whole droplet lifetime, indicating the importance of the interface for particle trapping and aggregation. The evaporation-induced radial flow carried along particles in the bulk toward the contact line. On the contrary, particle aggregates trapped at the LG interface were not affected by this flow, apart from the very last stages of the drying process when the drop thickness became comparable to the particle size. It has to be noted that once adsorbed at the LG interface, particles remained there, since the energy required for desorption is ~10^5 times larger than the thermal energy.[35] After evaporation was finished, a quite homogeneous deposit

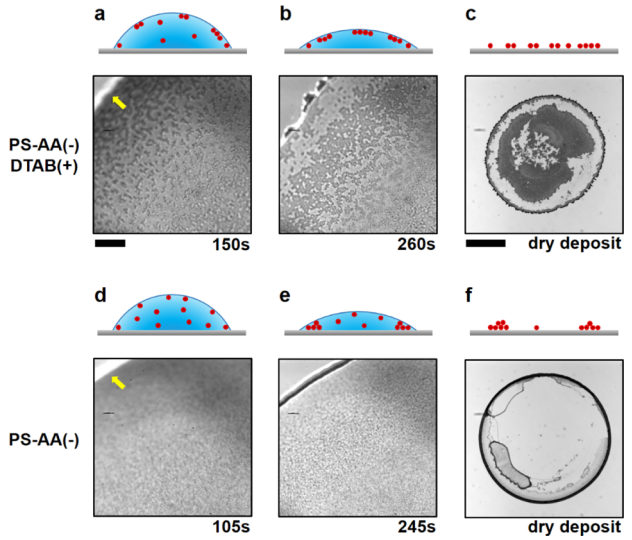

Figure 5. High-magnification snapshots during the evaporation of a drop (0.5 μL) containing anionic PS particles (PS-AA, 500 nm diameter, 1 mg/mL concentration) with (a,b) and without (d,e) 0.025 mM DTAB. The focal plane was kept at the drop liquid−gas (LG) interface in order to observe the behavior of particles there. Due to its curved shape, only a part of the LG interface was in-focus (roughly in the middle of the field of view). The drop contact line (indicated with a yellow arrow) was out of focus. The final dry deposits are shown at low magnification (c,f). For the drop containing DTAB, particle clusters accumulated at the interface (a) and formed later a dense particle skin (b), the deposition of which led to a fairly homogeneous pattern (c). For the surfactant-free drop, particle adsorption at the LG interface is much weaker (d), whereas at longer drying times no significant aggregation or network formation was observed (e). The dry pattern was thus a typical coffee ring (f). The scale bars are 50 and 500 μm for the high- (a,b and d,e) and low-magnification (c,f) images, respectively.

was obtained, comprising a ring encircling the deposited particle skin that was previously formed. Note that the obtained dry deposit (Figure 5c) displayed large empty areas compared to the deposits shown in Figure 1, which is attributed to the lower particle concentration used for this series of experiments. When the experiments were repeated at the same concentrations as in Figures 1 and 2 (2 mg/mL), a similar behavior was observed: flow of particles toward the contact line and formation of a ring-shaped pattern without surfactants, particle trapping at LG interface and disk formation in the presence of DTAB (Figure S5, Videos S3−S4). In this case, the disk pattern was more homogeneous and similar to the deposits shown in Figures 1 and 2.

In contrast, for the DTAB-free droplet, no aggregation in the bulk or at the LG interface was observed during evaporation (Figure 5d,e). This clearly indicates the role of the surfactant in enhancing particle affinity for the LG interface. In the absence of DTAB, particles were hydrophilic due to the acrylic acid groups on their surface and were thus preferably dispersed in the water phase rather than accumulating at the LG interface. In this case, particles were transported by the evaporation-driven radial outward flow toward the contact line and were gathered at the drop edge to form a typical ring pattern (Figure 5f).

Particle/Surfactant Mixtures: A General Picture. In this section, we summarize our observations on deposits formed by evaporating droplets of colloidal suspensions containing surfactants, and we suggest a general pattern formation

DOI: 10.1021/acs.langmuir.5b00453
Langmuir 2015, 31, 4113−4120

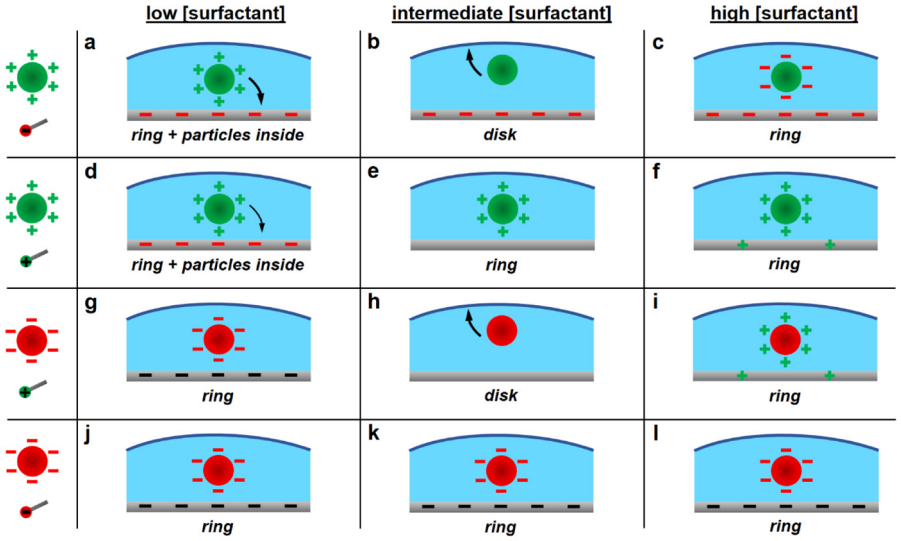

Figure 6. Role of particle−interface interactions on the formation of patterns from drops of surfactant−particle mixtures. For low surfactant concentrations, particles maintain their initial surface charge, either due to the low amount of adsorbed surfactants (oppositely charged systems) or negligible surfactant adsorption (like-charged systems). In this concentration region, electrostatic interactions between the particles and the substrate dictate the dry pattern morphology. Electrostatic repulsion leads to marked ring-shaped deposits (g,j), whereas attraction between oppositely charged particles and the LS interface also result in rings but with a significant number of particles deposited in the area enclosed by the ring (a,d). For intermediate surfactant concentrations, surfactant-mediated electrostatic as well as hydrophobic interactions define the deposit morphology. For oppositely charged systems, particles become neutral and hydrophobic and are trapped at the LG interface. Particle aggregation and skin formation in this case yield homogeneous disks (b,h). For like-charged systems, surfactants do not affect the particle surface properties; particles experience no attraction by the LG or LS interfaces, and the dry deposits are rings (e,k). For high surfactant concentrations, particle charge reverses in oppositely charged systems (c,i), while particles maintain their original charge for like-charged systems (f,l). Ring-shaped deposits are always formed.

mechanism governed by the interactions of particles with the LG and LS interfaces. We start with mixtures of cationic particles and anionic surfactants. For zero and low surfactant concentrations (Figure 6a), the particles remained plain or were partially decorated with surfactants, that is, they possessed a strong or intermediate positive charge. The electrostatic attraction between the negatively charged glass and the positively charged particles dominated. Therefore, even though most of the particles were transported to the contact line due to the radial evaporation-driven capillary flow, particles in proximity to the LS interface were attracted and immobilized there. The dry pattern was a ring with a significant number of particles within the pattern interior. For intermediate surfactant concentrations (Figure 6b), electrostatically driven adsorption of surfactants onto the particles rendered the latter nearly neutral and hydrophobic, owing to the fact that surfactant apolar tails were exposed to water. Particles acquired an enhanced affinity to the LG interface and got trapped there. Trapped particles were connected to each other to form a skin, which was unaffected by the radial capillary flow for most of the evaporation process. The dry pattern was therefore a homogeneous disk. For high surfactant concentrations (Figure 6c), surfactant assembly by hydrophobic interactions onto the particle surface led to an excess of surfactants and a reversal of the particle charge. Particles were again hydrophilic, since the polar surfactant heads pointed out from the particle surface. The capillary outward flow led to the formation of a typical ring deposit with almost no particle deposition in the interior due to the electrostatic repulsion by the LS interface.

Next, we focus on the case of cationic particles in the presence of cationic surfactants. For zero and low surfactant concentrations (Figure 6d), the glass substrate was either strongly or partially negative, due to no or partial surfactant adsorption. The plain cationic particles were attracted by the oppositely charged LS interface. Therefore, most of the particles were transported to the contact line due to the radial capillary flow; however, particles that were located close to the substrate were attracted and immobilized there. The dry pattern was a ring with a significant number of particles within. For intermediate surfactant concentrations (Figure 6e), particles remained cationic, while the glass substrate became neutral. Therefore, particles were not attracted to the LS interface, and most of them were carried along by the radial capillary flow, forming a typical ring-shaped pattern. The situation was similar for even higher surfactant concentrations (Figure 6f), except for the fact that the substrate could effectively become cationic due to adsorption of a surfactant bilayer.[36] A typical ring pattern was again observed, where the majority of the suspended particles gathered at the drop contact line. Note that the decrease in particle adsorption on the LS interface described in Figure 6e,f was observed for [CTAB] > 0.02 mM and [DTAB] > 0.1 mM (not shown in Figure 3) and was also frequently accompanied by a depinning of the contact line.

The general picture remained the same when suspensions of anionic particles were used. When cationic surfactants were added at low concentrations (Figure 6g), particles remained anionic, as few surfactants adsorbed on their surface. Similarly, minute surfactant adsorption to the glass surface left the LS interface negatively charged. Therefore, almost all particles were dragged to the drop edge by the capillary flow and a typical ring-shaped pattern was formed. At intermediate concentrations (Figure 6h), particles turned to neutral and hydrophobic and tended to adsorb at the LG interface, leading to the skin formation and a disk-shaped pattern after drop drying. Adsorption of surfactants at the LS interface presumably turned the glass neutral and hydrophobic too, which could lead to particle trapping there; however, this effect was not observed to

DOI: 10.1021/acs.langmuir.5b00453
Langmuir 2015, 31, 4113−4120

be strong. As surfactant concentration increased further (Figure 6i), the charge was reversed and probably the same happened to the substrate, both becoming positively charged. The resulting repulsive interaction did not favor particle adsorption at the LS interface; a classical ring-shaped deposit was thus formed. Finally, for anionic particle/anionic surfactant mixtures, surfactants were repelled by the particle surface groups, and thus no significant amount was adsorbed, for all surfactant concentrations (Figure 6j–l). Particles were therefore mostly dispersed in the bulk and were carried along with the radial flow; a typical ring-shaped pattern was formed for all surfactant concentrations.

A similar phenomenology was observed when larger anionic polystyrene particles with different surface chemistry were mixed with oppositely charged surfactants. Suspensions containing 1.1 and 3.6 μm particles having carboxyl surface groups led to rings, disk-shaped deposits and rings again with an increase in DTAB concentration. These results are preliminary, and more experiments are required for a clear understanding; however, they indicate that the observed pattern homogenization at intermediate surfactant concentration might be a generic effect for oppositely charged mixtures, irrespective of the detailed physicochemical properties of the colloids employed.

Considering the pattern homogenization mechanism, it is worth mentioning how surfactant-decorated particles reach the LG interface to get trapped there until final deposition. As discussed previously, a small number of particle aggregates could be observed at the LG interface, soon after drop deposition (~10 s). These aggregates are presumably created directly upon drop formation when a new LG interface is created. After drop deposition, both the number and the size of these aggregates increase with increasing evaporation time (Figure 5 and Videos S1–S4). It is thus interesting to consider by which mechanism particles can be transported at the LG interface. One possible candidate is a diffusive transport. For a 500 nm particle and for T = 20 °C, the diffusion coefficient calculated by the Stokes–Einstein equation is $D = 8.6 \times 10^{-13}$ m^2/s. For an evaporation time of ~390 s (typical value for 0.5 μL drops), the maximum displacement is Δx = 45 μm. Therefore, only a small number of particles could reach the LG interface by diffusion, and diffusive transport alone cannot accumulate enough particles to form the dense particle skin we observed at the LG interface. A second mechanism is the sweeping of particles by LG interface, which moves down upon evaporation. We think that it is the dominant mechanism, since the moving interface can eventually come in contact with all the particles, except the ones that are immobilized at the LS interface or at the contact line. Other transport mechanisms can be involved. For instance, both convective and Marangoni flows, if present, can dynamically reconfigure particle distribution inside the drop and at the vicinity of the LG interface and therefore affect the kinetics of particle trapping at this interface.

IV. CONCLUSIONS

In summary, we have examined the deposition patterns formed after the drying of microliter sessile drops from particle/surfactant mixtures (at concentrations below the CMCs) on glass substrates. For like-charged systems, dry patterns were always rings. For mixtures where colloids and surfactants possessed opposite charges, three pattern regions were revealed. For zero and low surfactant concentrations, ring-shaped deposits were formed after drying. For intermediate surfactant concentrations, the final patterns were homogeneous disks. Finally, for high surfactant concentrations, the dry patterns were again rings. The resulting deposit morphologies were explained on the basis of surfactant adsorption on the particle surface driven by both Coulomb and hydrophobic interactions and its critical role in modulating the interaction of the particles with the LS and LG interfaces. When particles became neutral and hydrophobic due to surfactant adsorption, their affinity to the LG interface of the evaporating drop was enhanced. Particle trapping and subsequent percolation at the LG interface led to the formation of a particle skin, which remained unaffected by the capillary radial outward flow, up to the very late stage of evaporation. The deposition of this skin led to the formation of homogeneous disks. In other cases, ring-shaped deposits were always formed, and the amount of particles deposited in the area enclosed by the ring was affected by the electrostatic interactions between the colloids and the LS interface.

The observed ring-disk-ring evolution with increasing surfactant concentration appears to be a universal effect leading to homogeneous deposits from drops of oppositely charged surfactant-particle mixtures. Contrarily to the common but not always successful method of using high surfactant concentrations to drive homogeneous particle deposition due to solutal Marangoni flows, the approach examined here involves surfactant addition at concentrations lower than the CMC. Its robust and generic character might provide a straightforward way to suppress the coffee-ring effect in applications of practical interest, such as in micropatterning and inkjet printing technologies.

In this paper, we have systematically analyzed the role of surfactants in directing particle deposition in evaporating drops. We have emphasized the determinant and primary role of surfactant-mediated particle interactions with the LS and LG interfaces. These results also raise new questions, especially regarding the mechanisms of particle transport to interfaces, which we think are worth being further explored. The evaporation rate seems to be an important parameter to be investigated, as it directly affects both the interface sweeping rate and the capillary-driven flows toward the contact line. Finally, the effect of surfactants on the contact line dynamics might also have a crucial role, as any transient or permanent depinnning of the contact line dramatically affects the deposition behavior.

■ ASSOCIATED CONTENT

Supporting Information

Height profiles of deposits formed from evaporating drops containing mixtures of anionic PS particles and DTAB at various surfactant concentrations; correlation between the zeta potential of anionic particle/surfactant mixtures and the deposits formed by evaporating drops of these mixtures; the effect of the interactions between the particles and the liquid–solid interface on deposit formation from drying suspensions; correlation between the zeta potential of cationic particle/surfactant mixtures and the deposits formed by evaporating drops of these mixtures; brightfield microscope images of the deposits formed from the evaporating drops used to record videos S3 and S4; four videos showing drop evaporation of anionic particle/cationic surfactant mixtures and anionic particle suspensions. This material is available free of charge via the Internet at http://pubs.acs.org.

DOI: 10.1021/acs.langmuir.5b00453
Langmuir 2015, 31, 4113–4120

AUTHOR INFORMATION

Corresponding Authors

*E-mail: emmanouil.anyfantakis@ens.fr.

*E-mail: damien.baigl@ens.fr. Phone: +33 1 4432 2405. Website: http://www.baigllab.com/.

Author Contributions

†These authors contributed equally to this work. M.A. and D.B. designed and supervised the work. M.A. and Z.G. performed all experiments and analyzed the data. M.A. and D.B. wrote the manuscript with contributions from all authors.

Notes

The authors declare no competing financial interest.

ACKNOWLEDGMENTS

We thank H. El-Deen Sharaf and U. Jonas for providing the anionic polystyrene nanoparticles, and C. Bain for fruitful discussion. This work was supported by the European Research Council (ERC) [European Community's Seventh Framework Programme (FP7/2007-2013)/ERC Grant agreement No. 258782 and FP7-PEOPLE-2013-IEF/Project 624806 "DIOPTRA"] and the Mairie de Paris [Emergence(s) 2012].

REFERENCES

(1) Deegan, R. D.; Bakajin, O.; Dupont, T. F.; Huber, G.; Nagel, S. R.; Witten, T. A. Capillary Flow as the Cause of Ring Stains from Dried Liquid Drops. *Nature* **1997**, *389*, 827−829.

(2) Deegan, R. D.; Bakajin, O.; Dupont, T. F.; Huber, G.; Nagel, S. R.; Witten, T. A. Contact Line Deposits in an Evaporating Drop. *Phys. Rev. E* **2000**, *62* (1), 756−765.

(3) Bhardwaj, R.; Fang, X. H.; Somasundaran, P.; Attinger, D. Self-Assembly of Colloidal Particles from Evaporating Droplets: Role of DLVO Interactions and Proposition of a Phase Diagram. *Langmuir* **2010**, *26* (11), 7833−7842.

(4) Larson, R. G. Transport and Deposition Patterns in Drying Sessile Droplets. *AIChE J.* **2014**, *60* (5), 1538−1571.

(5) Hu, H.; Larson, R. G. Marangoni Effect Reverses Coffee-Ring Depositions. *J. Phys. Chem. B* **2006**, *110*, 7090−7094.

(6) Fischer, B. J. Particle Convection in an Evaporating Colloidal Droplet. *Langmuir* **2002**, *18*, 60−67.

(7) Dugyala, V. R.; Basavaraj, M. G. Control over Coffee-Ring Formation in Evaporating Liquid Drops Containing Ellipsoids. *Langmuir* **2014**, *30*, 8680−8686.

(8) Majumder, M.; Rendall, C. S.; Eukel, J. A.; Wang, J. Y. L.; Behabtu, N.; Pint, C. L.; Liu, T.; Orbaek, A. W.; Mirri, F.; Nam, J.; et al. Overcoming the "Coffee-Stain" Effect by Compositional Marangoni-Flow-Assisted Drop-Drying. *J. Phys. Chem. B* **2012**, *116* (22), 6536−6542.

(9) Chhasatia, V. H.; Joshi, A. S.; Sun, Y. Effect of Relative Humidity on Contact Angle and Particle Deposition Morphology of an Evaporating Colloidal Drop. *Appl. Phys. Lett.* **2010**, *97* (23), 231909.

(10) Yunker, P. J.; Still, T.; Lohr, M. A.; Yodh, A. G. Suppression of the Coffee-Ring Effect by Shape-Dependent Capillary Interactions. *Nature* **2011**, *476* (7360), 308−311.

(11) Park, J.; Moon, J. Control of Colloidal Particle Deposit Patterns within Picoliter Droplets Ejected by Ink-Jet Printing. *Langmuir* **2006**, *22* (8), 3506−3513.

(12) Ristenpart, W. D.; Kim, P. G.; Domingues, C.; Wan, J.; Stone, H. A. Influence of Substrate Conductivity on Circulation Reversal in Evaporating Drops. *Phys. Rev. Lett.* **2007**, *99* (23), 234502.

(13) Le Berre, M.; Chen, Y.; Baigl, D. From Convective Assembly to Landau−Levich Deposition of Multilayered Phospholipid Films of Controlled Thickness. *Langmuir* **2009**, *25* (5), 2554−2557.

(14) Diguet, A.; Le Berre, M.; Chen, Y.; Baigl, D. Preparation of Phospholipid Multilayer Patterns of Controlled Size and Thickness by Capillary Assembly on a Microstructured Substrate. *Small* **2009**, *5*, 1661−1666.

(15) Calvert, P. Inkjet Printing for Materials and Devices. *Chem. Mater.* **2001**, *13*, 3299−3305.

(16) Blossey, R.; Bosio, A. Contact Line Deposits on cDNA Microarrays: A "Twin-Spot Effect. *Langmuir* **2002**, *18* (7), 2952−2954.

(17) Larson, R. G. Re-Shaping the Coffee Ring. *Angew. Chem., Int. Ed.* **2012**, *51*, 2546−2548.

(18) Cui, L.; Zhang, J.; Zhang, X.; Huang, L.; Wang, Z.; Li, Y.; Gao, H.; Zhu, S.; Wang, T.; Yang, B. Suppression of the Coffee Ring Effect by Hydrosoluble Polymer Additives. *ACS Appl. Mater. Interfaces* **2012**, *4* (5), 2775−2780.

(19) Talbot, E. L.; Yang, L.; Berson, A.; Bain, C. D. Control of the Particle Distribution in Inkjet Printing through an Evaporation-Driven Sol-Gel Transition. *ACS Appl. Mater. Interfaces* **2014**, *6* (12), 9572−9583.

(20) Deegan, R. Pattern Formation in Drying Drops. *Phys. Rev. E* **2000**, *61* (1), 475−485.

(21) Kajiya, T.; Kobayashi, W.; Okuzono, T.; Doi, M. Controlling the Drying and Film Formation Processes of Polymer Solution Droplets with Addition of Small Amount of Surfactants. *J. Phys. Chem. B* **2009**, *113* (47), 15460−15466.

(22) Deng, Y.; Zhu, X.-Y.; Kienlen, T.; Guo, A. Transport at the Air/water Interface Is the Reason for Rings in Protein Microarrays. *J. Am. Chem. Soc.* **2006**, *128* (9), 2768−2769.

(23) Still, T.; Yunker, P. J.; Yodh, A. G. Surfactant-Induced Marangoni Eddies Alter the Coffee-Rings of Evaporating Colloidal Drops. *Langmuir* **2012**, *28* (11), 4984−4988.

(24) Sempels, W.; De Dier, R.; Mizuno, H.; Hofkens, J.; Vermant, J. Auto-Production of Biosurfactants Reverses the Coffee Ring Effect in a Bacterial System. *Nat. Commun.* **2013**, *4*, 1757.

(25) Truskett, V.; Stebe, K. J. Influence of Surfactants on an Evaporating Drop: Fluorescence Images and Particle Deposition Patterns. *Langmuir* **2003**, *19* (20), 8271−8279.

(26) Yan, Q.; Gao, L.; Sharma, V.; Chiang, Y.-M.; Wong, C. C. Particle and Substrate Charge Effects on Colloidal Self-Assembly in a Sessile Drop. *Langmuir* **2008**, *24* (20), 11518−11522.

(27) Crivoi, A.; Duan, F. Amplifying and Attenuating the Coffee-Ring Effect in Drying Sessile Nanofluid Droplets. *Phys. Rev. E* **2013**, *87* (4), 042303.

(28) Anyfantakis, M.; Baigl, D. Dynamic Photocontrol of the Coffee-Ring Effect with Optically Tunable Particle Stickiness. *Angew. Chem., Int. Ed.* **2014**, *53*, 14077−14081.

(29) Vogel, N.; de Viguerie, L.; Jonas, U.; Weiss, C. K.; Landfester, K. Wafer-Scale Fabrication of Ordered Binary Colloidal Monolayers with Adjustable Stoichiometries. *Adv. Funct. Mater.* **2011**, *21* (16), 3064−3073.

(30) Fuguet, E.; Ràfols, C.; Rosés, M.; Bosch, E. Critical Micelle Concentration of Surfactants in Aqueous Buffered and Unbuffered Systems. *Anal. Chim. Acta* **2005**, *548* (1−2), 95−100.

(31) Biswas, S. C.; Chattoraj, D. K. Polysaccharide−Surfactant Interaction. 1. Adsorption of Cationic Surfactants at the Cellulose−Water Interface. *Langmuir* **1997**, *13* (17), 4505−4511.

(32) Deleurence, R.; Parneix, C.; Monteux, C. Mixtures of Latex Particles and the Surfactant of Opposite Charge Used as Interface Stabilizers - Influence of Particle Contact Angle, Zeta Potential, Flocculation and Shear Energy. *Soft Matter* **2014**, *10* (36), 7088−7095.

(33) Furton, K. G.; Norelus, A. Determining the Critical Micelle Concentration of Aqueous Surfactant Solutions: Using a Novel Colorimetric Method. *J. Chem. Educ.* **1993**, *70* (3), 254.

(34) Binks, B. P.; Rodrigues, J. A.; Frith, W. J. Synergistic Interaction in Emulsions Stabilized by a Mixture of Silica Nanoparticles and Cationic Surfactant. *Langmuir* **2007**, *23* (7), 3626−3636.

(35) Binks, B. P. Particles as Surfactants - Similarities and Differences. *Curr. Opin. Colloid Interface Sci.* **2002**, *7*, 21−41.

(36) Tyrode, E.; Rutland, M. W.; Bain, C. D.; Soc, J. A. C.; Asap, A. Adsorption of CTAB on Hydrophilic Silica Studied by Linear and Nonlinear Optical Spectroscopy Adsorption of CTAB on Hydrophilic Silica Studied by Linear and Nonlinear Optical Spectroscopy. *J. Am. Chem. Soc.* **2008**, *8* (33), 17434−17445.

DOI: 10.1021/acs.langmuir.5b00453
Langmuir 2015, 31, 4113−4120